JETIR.ORG ISSN: 2349-5162 | ESTD Year : 2014 | Monthly Issue
JOURNAL OF EMERGING TECHNOLOGIES AND INNOVATIVE RESEARCH (JETIR)
An International Scholarly Open Access, Peer-reviewed, Refereed Journal

SPECKLE NOISE REDUCTION IN SAR IMAGES USING HYBRID WAVELET FILTER WITH BIVARIATE SHRINKAGE FUNCTIONS

[1]Keerti Rai, [2]Avinash Rai, [3]AafreenAlam

[1]Department of EEE, Arka Jain University, Jamshedpur,Jharkhand
[2,3]UIT Rajiv Gandhi Proudyogiki Vishwavidyalaya, Gandhi Nagar, Bhopal, M.P
[3] MTech Scholar, [2]Assitant Professor [3] Assistant Professor
Email: aafreenalam28@gmail.com; avinashrai@rgtu.net; dr.keerti@arkajainuniversity.ac.in

Abstract : Recently, in many applications, Synthetic Aperture Radar (SAR) images play a very important role to visualize and observe scenarios. But, due to presence of speckle noise, SAR images are difficult to analyze as it degrades the quality of image and results in wrong interpretation. Speckle noise has characteristics of multiplicative noise. From last few years, researchers have focused their work for speckle noise reduction or despeckling. However, loss of edge information was observed in most of the existing works. Therefore, this paper is dedicated to design an algorithm for speckle reduction using benefits of wavelet transform and bivariate shrinkage functions. In the proposed algorithm first of all logarithmic transformation was performed to convert multiplicative noise to additive noise and further Lee filter is applied. Then filtered image was decomposed using wavelet transform. Further the bivariate shrinkage function was applied to estimate each coefficient and in last median filter was applied. The result analysis is performed on different test images and SAR images also. The result was evaluated on number of parameters such as Peak Signal to Noise Ratio (PSNR),Root Mean Square Error (RMSE), Structural Similarity (SSIM),Equivalent Number of Looks (ENL), Natural Image Quality Evaluator (NIQE) difference and time at different noise variance levels. The simulation result shows that the proposed algorithm outperforms better as compared to existing work and some conventional methods.

Keywords – **Additive White Gaussian Noise (AWGN)**, ***Bivariate Shrinkage, Discrete Wavelet Transform (DWT), Speckle Noise, Synthetic Aperture Radar (SAR),Wavelet Filter***

I. INTRODUCTION

While compared to optical remote sensing, synthetic aperture radar (SAR) sensors have quite numerous benefits, the most notable of which is the process of being able to capture for the whole day in every season [1]. The biggest disadvantage of SAR pictures, meanwhile, is the presence of speckle noise; it is a kind of undesirable or unwanted modification signal-related granular noise [2]. Numerous SAR image de-noising techniques were proposed over the last three decades. To tackle the issue, several researchers consider a significant loss of picture resolution as price but average a fixed set of different photos. The logarithmic transformation used initially reduce speckle noise approaches to generate an additive model that is simpler to work with. Subsequently, to work also with the changed model, certain well-known approaches for removing distortion, additive white Gaussian noise (AWGN) may be utilized as a reference [3]. Despite their ease of implementation, such techniques frequently overlook a few simple speckle properties. The log-transformed speckle interference, it does not precisely follow the zero mean Normal Distribution or known as the Gaussian distribution in practice. As a result, the variance must be righted before further processes start [4]. During the same era, highly complex algorithms relying upon that multiplicative speckle paradigm addressed de-noising inside this original domain. Such research papers demonstrated that a certain type of local adaptation is required to explain this image's nonstationary. With advancement as well as refinement of such multi-scale analysis framework, additional strategies for removing distortion as in the transform domain are becoming available. Wavelet shrinkage could be easily added to such transformed coefficients after homomorphic filtering. Wavelet methodologies, in addition to the spatial domain, enjoy the benefits of spatial adaptivity while altering for enhancing the image to effectively keep image textures but also boundaries [5]-[8].

Some researchers have put so much work into SAR images to remove speckle noise over the last several years, and a lot of approaches have been developed, including the Lee filter [5], the Kuan filter [6], the Frost filter [7], as well as the maximum a posteriori (MAP) filter [9]. Conventional spatial domain approaches, on the other hand, sometimes impair picture spatial quality but are also likely to over smooth aspects like corners as well as texturing. Such filter methods are relatively easy, but they do not maintain picture features like brightness, strength, edges, borders, etc., and overall system performance probably depends on the terrain of relevance. Subsequently, in recent times, transform domain filters like wavelet transform [8], [9], curvelet transforms [10], [11], as well as shearlet transform [12], [13] have been created and have obtained outstanding results. Whereas transform domain approaches efficiently reduce speckle, but also have flaws in backscatter preservation in some areas as well as detailed preservation within other regions, as well as the potential to induce pixel distortion and false defects. This is mostly owing to the

transform domain's intrinsic inefficiency, notwithstanding the image's valuable local or global qualities. To address the aforementioned difficulties, numerous approaches rely on the nonlocal mean (NLM) to replace a pixel's color with an average of the colors of nearby pixels. The most comparable pixels to a particular pixel, on the other hand, do not need to be near approach have been presented, which makes use of the picture's self-similarity by picking similar pixels in such an enlarged search field depending on patch wise similarity. Studies have extensively introduced the nonlocal low-rank model (NLRM)-relying on despeckling approaches [14], [15]. The multiscale nonlocal low-rank model NLRM is further improved by picking comparable

patches from various scales of the SAR picture while concurrently investigating the nonlocal low-rank model with multiscale prior [16][17]. Despite their great efficiency, Non-Local approaches need the calculation of a great amount of patch similarity measurements, resulting in a high computational effort. Because the distortion in the sub-bands has been in tiny coefficients while the features are in bigger coefficients, wavelet-focused speckle (distortion) removal has recently become very popular. Versatile signal processing tool Discrete wavelet transformations (DWT) were previously used to decrease speckle distortion in radar pictures. However, a key drawback of this tool is mainly in the transformation process, certain crucial image coefficients may be lost [18]. In speckle elimination, another approach called Non-Decimated Wavelet Transform (NDWT) was used to ameliorate the problem. Filling the interim gaps among decimation stages in discrete wavelet transformations DWT, which ultimately results inthe redundant and excessive depiction of decimated source information, is the crucial process. It ensures that in the 2 approaches discussed previously, discrete wavelet transformations (DWT) as well as Non-Decimated Wavelet Transform (NDWT), finding an optimal thresholding level is a critical job. Each method has its own set of benefits and drawbacks, but the wavelet filter is seen to be better than the others. To generate high-resolution synthetic aperture radar SAR pictures, this study proposes a wavelet-based bivariate shrinkage technique that delivers significant speckle reduction.

Several scholars have advocated thresholding wavelet coefficients to denoise a Synthetic Aperture Radar (SAR) image over the last two decades. SAR is a widely used method for getting high-resolution images. It's used in a variety of applications, including remote sensing, oceanography, geology, ecology, and interferometry. In this paper, the effectiveness of several speckle filters is explored. Researchers have found and effectively implemented a wavelet-based denoising technique for speckle removal in image data in recent years. Due to the restricted support of wavelet basis functions, wavelet transformation can efficiently characterize functions or signals with localized properties. After that, we remove speckle noise with a wavelet-based technique. Finally, we discovered that wavelet-based denoising outperforms traditional speckle filters.

This paper is prepared as follows; Section 2, Discusses the previous despeckling methods along with their performance. Section 3 discussed problem identification. Section 4 discusses the research methodology adopted in this paper. Section 5 discusses the performance result of the proposed model alongwith the quality matrices. Section 6 concludes the paper.

II. RELATED WORK

Castaneda et al. [19] proposed a hybrid median–mean filter (HM2F), a single-shot image computerized algorithms technique for reducing granular interference like speckle noise that is focused on the averaging of traditional median-filtered pictures with varied kernel sizes. Khare et al. [20] suggested a wavelet-based hybrid approach that relies on Non-local Means (NLM) and Weighted Nuclear Norm Minimization (WNNM) to noise reduction speckle noise-damaged US pictures. The NLM filter's denoising functionality is just employed on the Discrete Wavelet transform's (DWT) approximation component. Furthermore, the proposed technique is superior to current de-noise speckle-noise algorithms in preserving edge and structural information during noise removal. Jain et al. [21] evaluated the classification accuracy of a DFT-focused speckle reduction framework with a Lee filter and also no filter. The results of the experiments suggest here that the framework may significantly enhance whole classification accuracy. Because the research was conducted on 3 different class labels, indications show a large gain, however, forest shows just a little gain. Yahia et al. [22] modified first of all the filter's choice, optimized their parameters, as well as enhanced the estimate of local statistics. Iterative minimum mean square error (IMMSE) filter's performance analysis of noise removal with spatial detail preservation is improved. The filtering performances had enhanced once the enhanced iterative filtering procedure initiated by algorithms Non-Local Mean NLM filter during some rounds. Rahimizadeh et al. [23] presented a novel speckle-adaptive Linear-minimum-mean-square-error (LMMSE) focused estimator to raise the efficiency of Ultrasound (US) noise removal by using the existence of duplicate structures in Ultrasound pictures. The suggested non-local Linear Minimum Mean Square Error (NLMMSE) estimate outperforms the traditional LMMSE estimator. The suggested methodology attempted to gather ideal materials was collected; but, in the additive noise, selecting the most comparable pixels might be difficult. For the removal of granular interference speckle noise in ultrasonic pictures, Jain et al. [24] employed wavelet transform potentials as well as thresholding. The suggested technique demonstrates a better increase with low variation of noise, but negligible or even no enhancement with a large variance of granular interference, according to the performance study using synthetic pictures. Singh et al. [25] proposed a novel approach for removing speckle Synthetic Aperture Radar (SAR) pictures that combine a local correlation ally focused merging of high-frequency coefficients in the Discrete Wavelet Transform (DWT) to noise thresholding. The decomposing level is determined by computing entropy on the structure of the input patch for each layer. The suggested approach is focused on the entropy variable with the fusing of high-frequency coefficients for selecting the decomposition stage in a two-dimensional Discrete Wavelet Transform. The low-frequency coefficients are left alone duringdecomposition, whereas the high-frequency coefficients are threshold utilizing two separate shrinkage algorithms. As a result, the high-frequency coefficients are subjected to Bayesian and Bivariate shrinking procedures. The enhanced high-frequency coefficients are merged using a local correlation-based technique after conducting two separate thresholding procedures. The correlation approach is used to determine the threshold value.

1. PROBLEM IDENTIFICATION

3.1 Speckle noise Model

Because synthetic aperture radar (SAR) suffers from speckle noise, image despeckling is critical. Directional smoothing with strong thresholding was presented as a solution to this issue.

$$G_{m,n} = (F_{m,n} \times X_{m,n}) + \varphi_{m,n} \quad (1)$$

Where, $G_{m,n}$ is the observed image, $F_{m,n}$ the real image, $X_{m,n}$ is the speckled distortion and, $\varphi_{m,n}$is termed as an additive component of granular interference. The variables n & m represent axial and lateral input images, respectively.

3.2 Noise in SAR (Synthetic Apertures Radar) Images

Speckled noise O (i,j) is characterized in SAR image processing as the product of two components: a noise-free SAR I (i,j) image and a speckled noise D (i,j)image.

$$O_{x,y} = I_{x,y} \times D_{x,y} \quad (2)$$

Where, $O_{x,y}$= Observed image, $I_{x,y}$= Real SAR image, and $D_{x,y}$= speckle noise, and *x,y* represents the spatial location coefficient indices.

2. METHODOLOGY

Noise present in SAR images is multiplicative and non-gaussian in nature and it is quite difficult to remove such noise as compared to Gaussian noise. The main reason for this is that noise variance changes with a change in intensity. Mathematically, this multiplicative noise is presented in eqn (3).

$$y(i,j) = x(i,j) \cdot n(i,j) \quad (3)$$

Where, $y(i,j)$ = Speckle image
$x(i,j)$ = Original image
$n(i,j)$ = non-gaussian noise

In most the cases, the noise with unknown variance σ^2 is assumed to be stationary. For evaluation of additive noise variance, logarithmic transformation is applied on $y(i,j)$ and mathematically represented as in eqn (4).

$$\ln(y(i,j)) = \ln(x(i,j)) + \ln(n(i,j)) \quad (4)$$

Further, ln $y(i,j)$ is applied on discrete wavelet transform (DWT) and then thresholding is performed. After inverse DWT is applied that results in a reverse to logarithmic operation as illustrated in fig 1. The flowchart of the entire work is represented in fig 2.

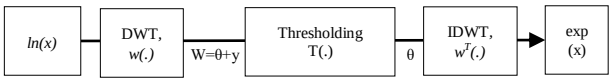

Fig. 1. Block diagram for denoising of speckle SAR image using logarithmic transformation

4.1 Symmetrical Boundary Extension

The denoising algorithm will involve symmetrical extension on the boundary of the original. Here, we propose to use symmetrical extension instead of zero padding to pad the image size to 512 pixels by 512 pixels because symmetrical boundary extension does not introduce significant distortion near the edges as zero padding. This approach is to extend the four sides of the original image before extending the remaining corners. The symmetric boundary extension is illustrated in fig 3.

4.2 Wavelet Decomposition

In this step, the image is decomposed into a wavelet and converted into 2D filter banks. The filter bank is applied to the row and column of the image. Two sub-bands, $N_1/2$ and N_2 are created by applying 1D filter bank analysis on each row and column. Then further, 1D analysis is applied to each sub-bands i.e., $N_1/2$ rows and $N_2/2$ columns, as shown in fig 4(a).

4.3 Perform Denoising

For denoising, threshold selection is performed. As illustrated in fig 4(b) 2D sampled wavelet transform is performed for creating sub band regions labeled as HH_k, HL_k, and LH_k. Here, scale is represented as $k$and j as the coarsest scale. With the smaller value of k, the scale is finer. The parent of sub-band S is represented as $P(S)$. From noisy wavelet coefficients, noise variance σ_n^2 is evaluated as stated in eqn (5) [1]:

$$\sigma_n^2 = \frac{Median(|y_i|)}{0.6745} \quad (5)$$

Where, y_{1i} is an element of sub-band $HH_1\sigma_{y1}$ and σ_{y2}can be found by :

$$\hat{\sigma}_{y1}^2 = \frac{1}{N_1^2} \sum_{y_{1i} \in s} y_{1i}^2 \quad (6)$$

$$\hat{\sigma}_{y2}^2 = \frac{1}{N_2^2} \sum_{y_{2i} \epsilon p(s)} y_{2i}^2 \quad (7)$$

Where $\sigma_{y1}$and σ_{y2} are Variances of $y_1$andy_2 . Using these variances signal variance σ_1&σ_2 can be estimated by applying the formula given:

$$\hat{\sigma}_1 = \sqrt{\hat{\sigma}_{y1}^2 - \hat{\sigma}_n^2} \quad (8)$$

$$\hat{\sigma}_2 = \sqrt{\hat{\sigma}_{y2}^2 - \hat{\sigma}_n^2} \quad (9)$$

Using bivariate shrinkage function

$$\hat{w}_1 = \frac{\left(\sqrt{y_1^2 + y_2^2} - \frac{\sqrt{3}\sigma_n^2}{\sigma}\right) + y_1}{\sqrt{y_1^2 + y_2^2}} \quad (10)$$

The algorithm is illustrated as:

1. Evaluate σ_n^2.
2. For each wavelet coefficient.
   a. Calculate σ_1, signal variance.
   b. Bivariate shrinkage function is applied tothe coefficient.

4.4 Wavelet Reconstruction

While in the reconstruction process, a filter bank is used. Sub-bands are combined using a 2D filter bank from N_1 and N_2.

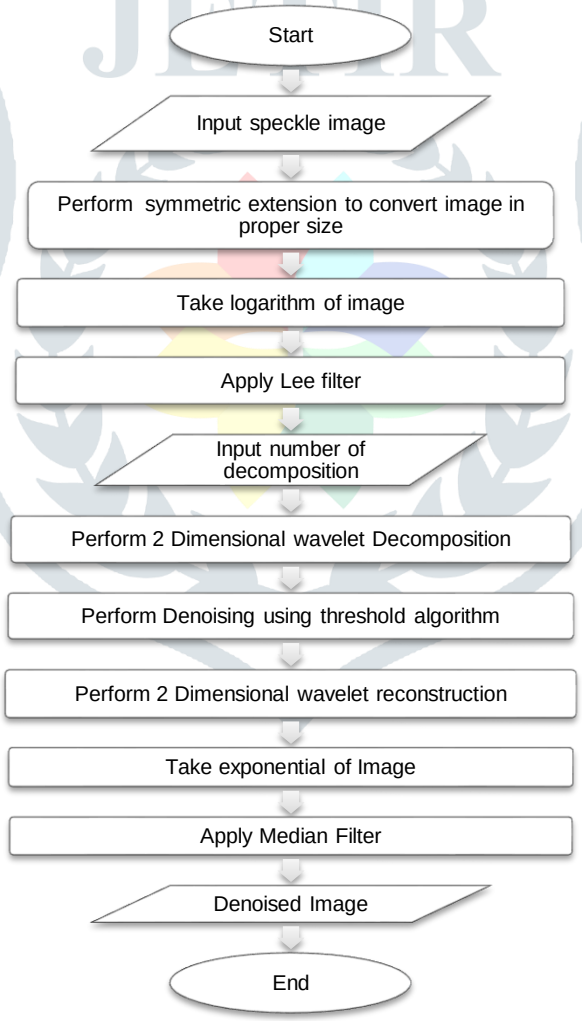

Fig. 2. Flowchart of proposed methodology

I =

X	X	X	X	X	X	X	X
X	X	X	X	X	X	X	X
X	X	1	2	3	4	X	X
X	X	5	6	7	8	X	X
X	X	9	0	A	B	X	X
X	X	C	D	E	F	X	X
X	X	X	X	X	X	X	X
X	X	X	X	X	X	X	X

Extends →

6	5	5	6	7	8	7	8
2	1	1	2	3	4	4	3
2	1	1	2	3	4	4	3
6	5	5	6	7	8	8	7
0	9	9	0	A	B	B	A
D	C	C	D	E	F	F	E
D	C	C	D	A	F	F	E
0	9	9	0	E	B	B	A

Fig. 3. Symmetrical Extension, (a) Before Boundary Extension, (b) After Boundary Extension

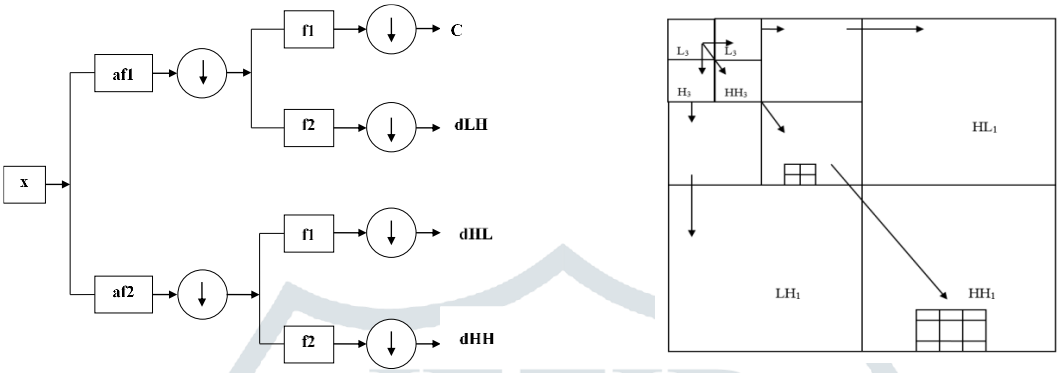

(a) One stage in multi-resolution wavelet decomposition of an image (b) Sub band regions of critically sampled wavelet transform.

Fig. 4. Wavelet Decomposition

3. RESULTS AND DISCUSSIONS

5.1 Quality Metrics

The performance of speckle reduction technologies is assessed using a variety of assessment metrics such as root mean square error (RMSE), peak signal to noise ratio (PSNR), structural similarity (SSIM), Equivalent Numbers of Looks, NIQE difference. All these parameters evaluate quality comparison among original and reconstructed image. For better quality assessment these parameters are quite necessary. These parameters are discussed as below:

Noise Variance: As more speckles are removed, a decreased variance results in a cleaner image. Eq. (11) contains the formula for computing variance.

$$\sigma^2 = \frac{1}{N}\sum_{j=0}^{N-1}(X_j)^2 \tag{11}$$

Root Mean Square Error (RMSE): RMSE is evaluated by calculating square root of error between reconstructed and original images. Higher value of RMSE means despeckling is not proper. Mathematically it is evaluated as in eqn. (12).

$$MSE = \sqrt{\frac{1}{N}\sum_{j=0}^{N-1}(X_j - \hat{X}_j)}^2 \tag{12}$$

Where, $X_j\hat{}$ = reconstructed image, X_j = original image and N = Size of the image.

Equivalent Numbers of Looks (ENL): Another performance parameter to evaluate speckle noise level is ENL. Higher the score, better the quality. Mathematically, ENL is evaluated as in eqn. (13):

$$ENL = \left(\frac{\mu}{\sigma}\right)^2 \tag{13}$$

Where μ is the mean of the uniform region and σ is the standard deviation of an uniform region.

Peak Signal to Noise Ratio (PSNR): The PSNR is most typically employed in image compression and de-noising as a measure of reconstruction quality. The acceptable average PSNR value is between 20-25db. The PSNR is calculated as:

$$PSNR = 10\log\left(\frac{255}{MSE}\right)^2 \tag{14}$$

So, as per eqn. (14), a higher PSNR value indicates better image speckle reduction. However, in this scenario, RMSE is higher for large speckle reduction.

NIQE_diff: The Natural Image Quality Evaluator (NIQE) is an performance measure that assess the image quality. The NIQE_diff is used to calculate the difference between the quality of an reconstructed/denoised image with respect to original image. A smaller score indicates better perceptual quality. Mathematically it is evaluated as in eqn. (15):

$$NIQE\_diff = NIQE(Original_{img}) - NIQE(Denoised_{img}) \tag{15}$$

Structural Similarity Index (SSIM): One of the quality assessment methodology in digital image processing is similarity. it is used to determine the comparison between images as well as videos. This index is completely reference based and determines the noisy or compressed or distorted images with some reference images. Therefore, to improve the performance of traditional methods such as peak signal-to-noise ratio (PSNR) and mean squared error (MSE), SSIM is designed. As higher the SSIM value more

structural similarity and less loss occurs in despeckling methods. The calculation of structural similarity formula with different window for measuring x1 and x2 of same size NxN is shown in equation (16):

$$SSIM\ (x1,x2) = \frac{(2\mu_1\mu_2+k_1)(2\sigma_{12}+k_2)}{(\mu_1^2+\mu_2^2+k_1)(\sigma_1^2+\sigma_2^2+k_2)} \qquad (16) \qquad (16)$$

Where, μ_1= mean of x, μ_2 = mean of, σ_{x1}^2 = variance of x1, σ_{x2}^2= variance of x2, σ_{x1x2}= co-variance of x1 and x2, k1 and k2 are variables to stabilize the separation with weak denominator.

5.2 Result Analysis

The reference images utilized in this study included the standard images for the 8-bit grey level (Lena, Boat, Cameraman, Airplane, Man, Peppers, and House), where we introduced speckle noise to each image to test the efficacy of the image noise reduction technique. The characteristics of multiplicative noise following the Rayleigh distribution were seen in these images. MATLAB (R2020) was used for all image processing. To evaluate the speckle-noise reduction performance, the proposed algorithm is compared to traditional filtering approaches such as Gaussian, Frost, SRAD, Bitonic filters, K-SVD and Preprocessing Filter, and Discrete Wavelet transform-based Noise Reduction Technique algorithm. Some of the test results of the proposed methodology are presented in fig 5.

The performance evaluation of the proposed methodology is presented in table 1. In table 1, PSNR, SSIM, ENL, NIQE_diff, and Time are taken as performance evaluation parameters. The analysis is presented on different input images and some of them are presented here. Five different images are observed and compared with different noise variance levels, i.e., 0.025 to 0.055. At a noise variance of 0.025, the highest PSNR (31.0099) was observed by 'cameraman' and ENL value (674.69) was observed by 'Lena' image and the lowest NIQE difference (0.7546) was observed in 'Lena' image. Whereas the highest SSIM (0.984) was observed by 'Nimes' image. The average time required to process these images was approx. 27 sec. Similarly, at a noise variance 0.035, the highest PSNR (30.39) was observed by 'cameraman' image. Whereas highest ENL (674.202) and lowest NIQE_diff (0.8465) were observed in 'Lena' image. Highest SSIM was 0.98329 for 'Nimes' image. Likewise, at a noise variance 0.045, the highest PSNR (29.4199) was observed in 'cameraman' image, and highest SSIM (0.98026) was observed in 'Nimes' image. Whereas highest ENL (675.2305) and lowest NIQE_diff (0.7798) was observed in 'Lena' image. Likewise, at noise variance 0.055, the highest PSNR (29.2236) was observed in 'cameraman' image, and the highest SSIM (0.98026) was observed in 'Nimes' image. Whereas highest ENL (676.2234) and lowest NIQE_diff (0.9021) was observed in 'Lena' image.

Table 2 and Table 3 illustrate a comparison of the proposed wavelet-based bivariate shrinkage technique with different methods. Table 2 represents the RMSE, PSNR, and SSIM comparison among methods. The result illustrates that the proposed algorithm shows better PSNR on peppers images. This means the image shows the best noise reduction and shows better edge preservation. The PSNR of the given peppers image is 30.69 whereas the Frost filter shows the lowest PSNR of 23.28. However, the best RMSE and SSIM were observed to be 7.54 and 0.94 respectively of Man image, whereas maximum RMSE and minimum SSIM were of Frost filter i.e., 15.03 and 0.58 respectively. Similarly, table 3 represents ENL comparison among methods. Table 3 illustrates the ENL performance of a homogeneous region. The best ENL was observed to be 382.47 on the baseball diamond image of the proposed wavelet-based bivariate shrinkage filter. The minimum ENL was observed by frost filter i.e., 88.80. Similarly, the noise reduction in the homogeneous regions of the building image was 347.28 (proposed wavelet-based bivariate shrinkage filter) which was best compared to others. Due to over smoothing of Frost filter, this exhibits the least ENL i.e., 106.57.

For the developed method, the time complexity is considered as the computation burden issue. From the result analysis presented here, it is observed that the time complexity of the model is on an average 31sec. It has been achieved as a remarkable parameter that other existing work doesn't consider. In this paper, we have evaluated time complexity that further can be improvised as future scope.

In comparison to other typical filter methods, the Bivariate Shrinkage Function has the lowest noise variance. In the Bivariate shrinkage function, which measures picture smoothness, the highest number of Looks is obtained. In the bivariate technique, the mean square error is the highest. As a result, the disparity between the original and de-noised image is bigger. This indicates a significant reduction in speckle. When compared to speckle filters, the de-noised images and results from Table 2 show decisively that the wavelet-based bivariate shrinkage technique delivers significant speckle reduction. In contrast, it can be concluded that the proposed wavelet-based bivariate shrinkage outperforms best as compared to others and doesn't result in a blurring effect in the high-frequency regions of the image, and shows better edge preservation performance.

Table 1. Despeckling Performance Evaluation

Image	PSNR	SSIM	ENL	NIQE_diff	Time (in Sec)
Noise Variance =0.025					
Lena	30.0536	0.91838	674.6944	0.7546	27.1846
Cameraman	31.0099	0.89595	364.998	1.8968	27.1807
Nimes	25.591	0.98471	580.5259	1.4655	27.3899
SAR image1	26.1771	0.92874	849.4022	2.4867	27.3909
SAR image2	28.453	0.96349	824.3047	1.8221	27.2684
Noise Variance =0.035					
Lena	29.1732	0.8937	674.202	0.8465	31.2594
Cameraman	30.3924	0.86785	364.2668	1.9820	27.5813
Nimes	25.2442	0.97329	585.6637	1.6188	35.0847
SAR image1	25.894	0.89177	846.02	2.6132	26.5612
SAR image2	28.0456	0.95193	819.8086	2.0538	40.9221
Noise Variance =0.045					
Lena	28.5546	0.87244	675.2305	0.7798	27.2148
Cameraman	29.4199	0.84135	363.5747	1.9778	28.3358
Nimes	24.5676	0.97171	589.4473	1.5804	27.0331
SAR image1	25.5785	0.87432	843.5676	2.9462	26.5103
SAR image2	27.6781	0.94972	817.2391	2.1241	42.4072
Noise Variance =0.055					
Lena	27.5635	0.85437	676.2234	0.9021	27.5067
Cameraman	29.2236	0.81943	363.1804	1.9753	57.7786
Nimes	23.8172	0.96026	591.8856	1.7834	27.4445
SAR image1	25.318	0.85898	838.5294	2.9992	26.2621
SAR image2	27.48	0.94727	814.7924	2.3100	26.0796

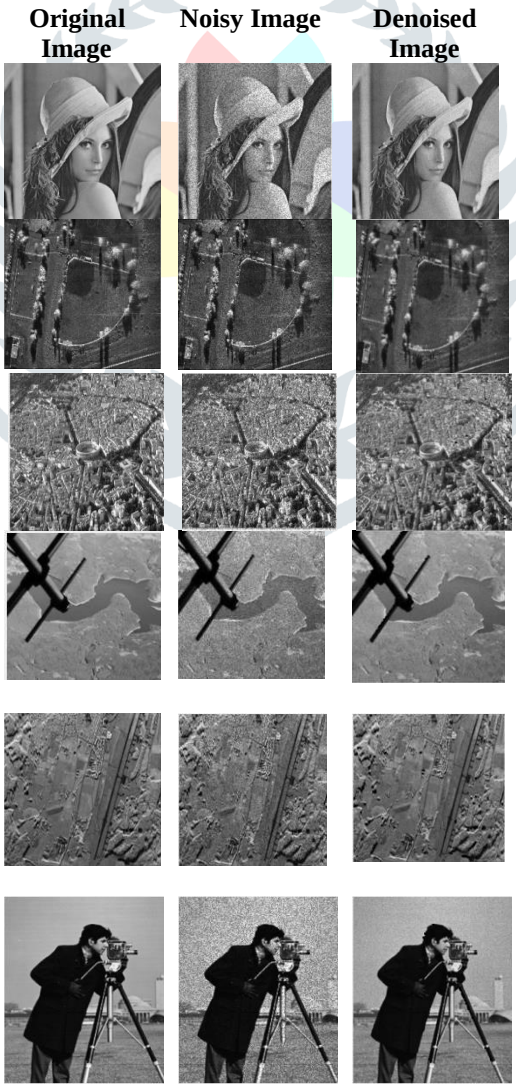

Fig.5 *The test images from top to bottom (Lena, SAR Baseball, Nimes, SAR image1, SAR image2 Cameraman, Boat, House, Man and Peppers), (left) original image, (centre) image under noise and (right) image after filtration.*

Table 2. Comparative Performance Analysis

Image (size)	Measure	Noisy	Gaussian	K-SVD	Frost	SRAD	Bitonic	Previous	Proposed
Lena (512 x 512)	RMSE	30.31	13.49	15.1	17.4	11.85	13.31	8.18	**7.89**
	PSNR (dB)	18.50	25.53	24.5	23.3	26.65	25.65	29.88	**29.95**
	SSIM	0.27	0.70	0.56	0.45	0.72	0.75	0.81	**0.89**
Boat (512 x 512)	RMSE	31.66	13.86	16.3	19.5	11.20	14.53	10.93	**8.82**
	PSNR (dB)	18.12	25.30	23.8	22.3	27.15	24.89	27.36	**28.23**
	SSIM	0.32	0.65	0.53	0.43	0.70	0.64	0.72	**0.91**
Cameraman (256 x 256)	RMSE	31.05	19.14	18.2	19.9	12.20	18.77	11.84	**8.34**
	PSNR (dB)	18.29	22.49	22.9	22.1	26.41	22.66	26.66	**28.70**
	SSIM	0.41	0.61	0.50	0.47	0.70	0.69	0.77	**0.87**
House (256 x 256)	RMSE	33.05	13.90	18.0	19.5	10.28	12.15	9.37	**9.13**
	PSNR (dB)	17.75	25.27	22.9	22.3	27.89	26.44	28.69	**28.92**
	SSIM	0.24	0.64	0.53	0.37	0.68	0.73	0.77	**0.85**
Man (1024x1024)	RMSE	24.68	10.81	13.5	15.0	8.83	11.76	8.63	**7.54**
	PSNR (dB)	20.28	27.45	25.5	24.5	29.21	26.72	29.41	**29.79**
	SSIM	0.47	0.73	0.62	0.58	0.77	0.70	0.79	**0.94**
Peppers (512 x 512)	RMSE	30.20	10.56	15.9	17.4	8.42	9.89	7.66	**8.35**
	PSNR (dB)	18.53	27.66	24.1	23.2	29.63	28.23	30.45	**31.64**
	SSIM	0.29	0.76	0.60	0.44	0.77	0.82	0.83	**0.91**
Airplane (512 x 512)	RMSE	38.53	14.17	23.7	21.0	11.77	14.19	11.06	**9.59**
	PSNR (dB)	16.42	25.10	20.6	21.6	26.71	25.09	27.26	**27.92**
	SSIM	0.20	0.67	0.34	0.35	0.68	0.75	0.81	**0.81**

Table 3. ENL Comparative Analysis

Measure	Noisy	Gaussian	K-SVD	Frost	SRAD	Bitonic	Previous	Proposed
ENL	31.41	163.82	340.33	88.80	156.74	260.18	246.17	**382.47**
	50.49	96.03	255.18	106.57	159.14	213.23	210.88	**347.28**

4. CONCLUSION

After result analysis some difficulties arised that are listed below:

- Time complexity is approx. 31sec which can further be reduced.
- Tested samples show an RMSE average of 8, which needs to be further reduced to lower the losses occurs in despeckling.
- PSNR value of tested samples was approx. 30db that can further be enhanced.

In this paper, wavelet transform is applied to scale as well as to remove speckle noise from the image and convert it into a multi-resolution representation. For this, the paper has adopted, a bivariate shrinkage function with a combination of wavelet decomposition at different noise variance levels. The result is evaluated on different performance parameters and compared with some existing techniques. Asa result, a more effective methodology can be developed. In future work, this work can be extended with dual-tree complex wavelet transform that can be used for multiresolution image denoising and de-blurring.

REFERENCES

[1] Castaneda, Raul, Jorge Garcia-Sucerquia, and Ana Doblas. "Speckle noise reduction in coherent imaging systems via hybrid median–mean filter." Optical Engineering 60, no. 12 (2021): 123107.

[2] Khare, Saurabh, and Praveen Kaushik. "Speckle filtering of ultrasonic images using weighted nuclear norm minimization in wavelet domain." Biomedical Signal Processing and Control 70 (2021): 102997.

[3] Jain, Vijal, Sanjay Shitole, Varsha Turkar, and Anup Das. "Impact of DFT Based Speckle Reduction Filter on Classification Accuracy of Synthetic Aperture Radar Images." In 2020 IEEE India Geoscience and Remote Sensing Symposium (InGARSS), pp. 54-57. IEEE, 2020.

[4] Yahia, Mohamed, Tarig Ali, Mohammad Maruf Mortula, Riadh Abdelfattah, Samy El Mahdy, and Nuwanthi Sashipraba Arampola. "Enhancement of SAR speckle denoising using the improved iterative filter." IEEE Journal of Selected Topics in Applied Earth Observations and Remote Sensing 13 (2020): 859-871.

[5] Rahimizadeh, Niloofar, Reza PR Hasanzadeh, and Farrokh Janabi-Sharifi. "An optimized non-local LMMSE approach for speckle noise reduction of medical ultrasound images." Multimedia Tools and Applications 80, no. 6 (2021): 9231-9253.

[6] Jain, Leena, and Palwinder Singh. "A novel wavelet thresholding rule for speckle reduction from ultrasound images." Journal of King Saud University-Computer and Information Sciences (2020).

[7] Singh, Prabhishek, Raj Shree, and Manoj Diwakar. "A new SAR image despeckling using correlation based fusion and method noise thresholding." Journal of King Saud University-Computer and Information Sciences 33, no. 3 (2021): 313-328.

[8] D. Guan, D. Xiang, X. Tang, and G. Kuang, "A SAR Image Despeckling Method Using Multi-Scale Nonlocal Low-Rank Model," IEEE Geosci. Remote Sens. Lett., vol. 17, no. 3, pp. 421–425, Mar. 2020, doi: 10.1109/LGRS.2019.2926196.

[9] D. Guan, D. Xiang, X. Tang, and G. Kuang, "SAR Image Despeckling Based on Nonlocal Low-Rank Regularization," IEEE Trans. Geosci. Remote Sens., vol. 57, no. 6, pp. 3472–3489, Jun. 2019, doi: 10.1109/TGRS.2018.2885089.

[10] A. G. Sujitha, D. P. Vasuki, and A. A. Deepan, "Hybrid Laplacian Gaussian Based Speckle Removal in SAR Image Processing," J. Med. Syst., vol. 43, no. 7, Jul. 2019, doi: 10.1007/S10916-019-1299-0.

[11] H. Choi and J. Jeong, "Despeckling images using a preprocessing filter and discrete wavelet transform-based noise reduction techniques," IEEE Sens. J., vol. 18, no. 8, pp. 3131–3139, Apr. 2018, doi: 10.1109/JSEN.2018.2794550.

[12] B. H. Wang, C. Y. Zhao, and Y. Y. Liu, "An improved SAR interferogram denoising method based on principal component analysis and the Goldstein filter," Remote Sens. Lett., vol. 9, no. 1, pp. 81–90, Jan. 2018, doi: 10.1080/2150704X.2017.1392633.

[13] G. Chen, G. Li, Y. Liu, X. P. Zhang, and L. Zhang, "SAR image despeckling by combination of fractional-order total variation and nonlocal low rank regularization," Proc. - Int. Conf. Image Process. ICIP, vol. 2017-September, pp. 3210–3214, Feb. 2018, doi: 10.1109/ICIP.2017.8296875.

[14] J. Geng, J. Fan, X. Ma, H. Wang, and K. Cao, "An iterative low-rank representation for SAR image despeckling," Int. Geosci. Remote Sens. Symp., vol. 2016-November, pp. 72–75, Nov. 2016, doi: 10.1109/IGARSS.2016.7729009.

[15] S. Liu, M. Shi, S. Hu, and Y. Xiao, "Synthetic aperture radar image de-noising based on Shearlet transform using the context-based model," Phys. Commun., vol. 13, no. PC, pp. 221–229, Dec. 2014, doi: 10.1016/J.PHYCOM.2014.02.002.

[16] B. Hou, X. Zhang, X. Bu, and H. Feng, "SAR image despeckling based on nonsubsampled shearlet transform," IEEE J. Sel. Top. Appl. Earth Obs. Remote Sens., vol. 5, no. 3, pp. 809–823, 2012, doi: 10.1109/JSTARS.2012.2196680.

[17] J. J. Ranjani and S. J. Thiruvengadam, "Dual-tree complex wavelet transform based sar despeckling using interscale dependence," IEEE Trans. Geosci. Remote Sens., vol. 48, no. 6, pp. 2723–2731, Jun. 2010, doi: 10.1109/TGRS.2010.2041241.

[18] D. Gleich, M. Kseneman, and M. Datcu, "Despeckling of terraSAR-X data using second-generation wavelets," IEEE Geosci. Remote Sens. Lett., vol. 7, no. 1, pp. 68–72, 2010, doi: 10.1109/LGRS.2009.2020610.

[19] F. Argenti, T. Bianchi, and L. Alparone, "Multiresolution MAP despeckling of SAR images based on locally adaptive generalized Gaussian pdf modeling," IEEE Trans. Image Process., vol. 15, no. 11, pp. 3385–3399, Nov. 2006, doi: 10.1109/TIP.2006.881970.

[20] P. Yan, C. Chen, and C. Chen, "An algorithm for filtering multiplicative noise in wide range Un algorithme pour le filtrage du bruit multiplicatif APPLICATIONS," 2005.

[21] A. Achim, P. Tsakalides, and A. Bezerianos, "SAR image denoising via Bayesian wavelet shrinkage based on heavy-tailed modeling," IEEE Trans. Geosci. Remote Sens., vol. 41, no. 8, pp. 1773–1784, Aug. 2003, doi: 10.1109/TGRS.2003.813488.
[22] D. T. Kuan, A. A. Sawchuk, T. C. Strand, and P. Chavel, "Adaptive Noise Smoothing Filter For Images With Signal-Dependent Noise.," IEEE Trans. Pattern Anal. Mach. Intell., vol. PAMI-7, no. 2, pp. 165–177, 1985, doi: 10.1109/TPAMI.1985.4767641.
[23] V. S. Frost, J. A. Stiles, K. S. Shanmugan, and J. C. Holtzman, "A Model for Radar Images and Its Application to Adaptive Digital Filtering of Multiplicative Noise," IEEE Trans. Pattern Anal. Mach. Intell., vol. PAMI-4, no. 2, pp. 157–166, 1982, doi: 10.1109/TPAMI.1982.4767223.
[24] J. Sen Lee, "Digital Image Enhancement and Noise Filtering by Use of Local Statistics," IEEE Trans. Pattern Anal. Mach. Intell., vol. PAMI-2, no. 2, pp. 165–168, 1980, doi: 10.1109/TPAMI.1980.4766994.

G. April and H. H. Arsenault, "Properties of speckle integrated with a finite aperture and logarithmically transformed," JOSA, Vol. 66, Issue 11, pp. 1160-1163, vol. 66, no. 11, pp. 1160–1163, Nov. 1976, doi: 10.1364/JOSA.66.001160.